Monthly Notices of the ROYAL ASTRONOMICAL SOCIETY

MNRAS **516,** 5309–5317 (2022) https://doi.org/10.1093/mnras/stac2332
Advance Access publication 2022 August 29

A follow-up on intermediate-mass black hole candidates in the second LIGO–Virgo observing run with the Bayes Coherence Ratio

Avi Vajpeyi [1,2]★ Rory Smith [1,2] Eric Thrane [1,2] Gregory Ashton [1,2,3] Thomas Alford,[4] Sierra Garza,[4] Maximiliano Isi [5] Jonah Kanner [4] T. J. Massinger[4] and Liting Xiao[4]

[1]*School of Physics and Astronomy, Monash University, Clayton VIC 3800, Australia*
[2]*OzGrav: The ARC Centre of Excellence for Gravitational Wave Discovery, Clayton VIC 3800, Australia*
[3]*Department of Physics, Royal Holloway, University of London, Egham TW20 0EX, United Kingdom*
[4]*LIGO Laboratory, California Institute of Technology, Pasadena, CA 91125, USA*
[5]*Center for Computational Astrophysics, Flatiron Institute, 162 5th Ave, New York, NY 10010, USA*

Accepted 2022 July 27. Received 2022 July 19; in original form 2021 August 5

ABSTRACT

The detection of an intermediate-mass black hole population (10^2–$10^6\,M_\odot$) will provide clues to their formation environments (e.g. discs of active galactic nuclei, globular clusters) and illuminate a potential pathway to produce supermassive black holes. Ground-based gravitational-wave detectors are sensitive to mergers that can form intermediate-mass black holes weighing up to $\sim 450\,M_\odot$. However, ground-based detector data contain numerous incoherent short duration noise transients that can mimic the gravitational-wave signals from merging intermediate-mass black holes, limiting the sensitivity of searches. Here, we follow-up on binary black hole merger candidates using a ranking statistic that measures the coherence or incoherence of triggers in multiple-detector data. We use this statistic to rank candidate events, initially identified by all-sky search pipelines, with lab-frame total masses $\gtrsim 55\,M_\odot$ using data from LIGO's second observing run. Our analysis does not yield evidence for new intermediate-mass black holes. However, we find support for eight stellar-mass binary black holes not reported in the first LIGO–Virgo gravitational wave transient catalogue GWTC-1, seven of which have been previously reported by other catalogues.

Key words: gravitational waves – methods: data analysis – methods: statistical – black hole mergers.

1 INTRODUCTION

Stellar mass ($M_{\rm BH} < 10^2\,M_\odot$) and supermassive black holes ($M_{\rm BH} > 10^6\,M_\odot$) have been observed and well-studied since the 1970s (Webster & Murdin 1972; Balick & Brown 1974; Ghez et al. 1998; Genzel, Eisenhauer & Gillessen 2010; Abbott et al. 2019b, 2021a; Event Horizon Telescope Collaboration et al. 2019). However, there is a deficiency of observational evidence for black holes in the intermediate-mass range $10^2 - 10^6\,M_\odot$. A variety of techniques have been employed to search for intermediate-mass black hole (IMBH) candidates including reverberation mapping (Peterson 2014), direct kinematic measurements (Schödel et al. 2002; Kızıltan, Baumgardt & Loeb 2017), applying macroscopic galaxy to black hole mass scaling relations, $M_{\rm BH}$–σ and $M_{\rm BH}$–L relations (Graham & Scott 2013; Wevers et al. 2017), studying X-ray luminosity and spectra (Greene & Ho 2004; Lin et al. 2020), gravitational lensing of gamma-ray burst light curves (Paynter, Webster & Thrane 2021), and others (see Koliopanos 2017; Mezcua 2017; Greene, Strader & Ho 2020). However, because IMBH have smaller masses than those of supermassive black holes, it is much more challenging to observe them with these observational techniques (Mezcua 2017). Additionally, numerous IMBH candidates discovered using these techniques are ambiguous as the observations can be attributed to other sources (e.g. light sources orbiting clusters of stellar-mass black holes, Ridolfi et al. 2016; Freire et al. 2017; anisotropic emission from neutron stars, Israel et al. 2017; Rodríguez Castillo et al. 2020). The discovery of an IMBH population will bridge the intermediate-mass observational gap, probe IMBH formation environments (e.g. accretion discs of active galactic nuclei, McKernan et al. 2012, 2014, 2018, 2019; Bellovary et al. 2016; Yang et al. 2019a,b; Gröbner et al. 2020; Ishibashi & Gröbner 2020; Samsing et al. 2022; Tagawa, Haiman & Kocsis 2020; Tagawa et al. 2021; the centres of dense stellar clusters, Romero-Shaw et al. 2020b; Anagnostou, Trenti & Melatos 2020; Martinez et al. 2020; Banerjee 2021a,b; Ballone et al. 2021; Bouffanais et al. 2021; Kumamoto et al. 2021; Mapelli et al. 2021; Weatherford et al. 2021; Zevin et al. 2021; Population-III stars, Inayoshi et al. 2017; Liu & Bromm 2020; Safarzadeh & Haiman 2020; Farrell et al. 2021; Toubiana et al. 2021), and illuminate our understanding of supermassive black hole formation (Gürkan, Fregeau & Rasio 2006; Amaro-Seoane et al. 2007; Arca Sedda & Mastrobuono-Battisti 2019; Askar, Davies & Church 2021).

Compact binary coalescences (CBCs) can provide gravitational-wave signals for IMBH candidates e.g. the $142^{+28}_{-16}\,M_\odot$ (90 per cent credible intervals) remnant observed from the gravitational-wave event GW190521 (Abbott et al. 2020c) and other candidates (Abbott et al. 2019a; Chandra et al. 2021; Abbott et al. 2022). As a binary's lab-frame total mass M is associated with its gravitational-wave merger frequency, $f \propto M^{-1}$, ground-based gravitational-wave detectors ($f \sim 10^1 - 10^3$ Hz) are sensitive to the last milliseconds of

★ E-mail: avi.vajpeyi@monash.edu

merging systems with $100\,M_\odot < M < 400\,M_\odot$ (LIGO Scientific Collaboration et al. 2015; Martynov et al. 2016; Moore, Cole & Berry 2014; Acernese et al. 2015), while space-based detectors ($f \sim 10^{-2}$–10^{1} Hz) can study the full signals of merging systems with $10^4\,M_\odot < M < 10^7\,M_\odot$ (Moore et al. 2014; Lu, Tan & Shao 2019). Because of the short duration of IMBH gravitational-wave signals in ground-based detectors, data quality is critical for their detection. Gravitational-wave data is characterized by numerous non-stationary terrestrial artifacts called *glitches* (Nitz 2018; Powell 2018; Cabero et al. 2019). Like signals from IMBH mergers, most glitches last for a fraction of a second, making them difficult to distinguish from astrophysical signals. These glitches can decrease the sensitivity of searches for binary black hole mergers with $M \gtrsim 55\,M_\odot$ (Nitz 2018).

Although a significant fraction of the glitches can be identified by testing them for coherence amongst two or more detectors and performing matched-filtering, these methods are insufficient to identify all glitches (Nitz 2018; Powell 2018; Cabero et al. 2019). One method to discriminate more glitches while searching for CBCs is the Bayesian odds (Veitch & Vecchio 2010; Kanner et al. 2016; Isi et al. 2018; Ashton, Thrane & Smith 2019b; Ashton & Thrane 2020; Pratten & Vecchio 2020). The Bayesian Coherence Ratio $\rho_{\rm BCR}$ (Isi et al. 2018; Ashton et al. 2019b) is a Bayesian odds comparing the probability that the data contains coherent signals versus incoherent glitches. In this paper, we use the $\rho_{\rm BCR}$ to rank O2's coincident CBC gravitational-wave candidates with lab-frame total masses in the range of $55 - 500\,M_\odot$. We present the candidates' $p_{\bar{B}}$, the probability that the candidate is inconsistent with the background distributions of $\rho_{\rm BCR}$ values computed from time-slid data. Additionally, for comparison, we provide the candidate's $p_{\rm astro}$ values reported by the LIGO-Virgo-KAGRA (LVK) collaboration in GWTC-1 (Abbott et al. 2019b), the PyCBC-team (Allen 2005; Allen et al. 2012; Dal Canton et al. 2014; Usman et al. 2016; Nitz et al. 2017,2018, 2020a, c, b; Davies et al. 2020), by the Institute of Advanced study's team (IAS; Venumadhav et al. 2019; Zackay et al. 2021), and by Pratten & Vecchio (2020).

We find that (a) events reported in GWTC-1, including GW170729 (likely the most massive BBH system in GWTC-1) are statistically significant $p_{\bar{B}} > 0.9$; (b) three out of the eight IAS events and candidates have $p_{\bar{B}} > 0.9$, corroborating IAS's detection claims for GW170304, GW170727, and GW170817A; and that (c) our ranking statistic does not identify any new IMBH, but does identify an unreported marginal stellar mass binary black hole candidate, 170222 with $p_{\bar{B}} \sim 0.6$.[1]

The remainder of this paper is structured as follows. We outline our methods, including details of our ranking statistic and the retrieval of our candidates in Section 2. We present details on the implementation of our analysis in Section 3. Finally, we present our results in Section 4 and discuss these results in the context of the significance of gravitational-wave candidates in Section 5.

2 METHOD

2.1 A Bayesian ranking statistic

The standard framework to identify CBC gravitational-wave signals in data is to quantify the significance of candidates with null-hypothesis significance testing (Abbott et al. 2019b, 2021a). In this framework, the candidates' ranking statistic is compared against a background distribution. The independent matched-filter searches, e.g. PyCBC (Usman et al. 2016), SPIIR (Chu et al. 2022) and GstLAL (Sachdev et al. 2019), and Coherent WaveBurst (Klimenko et al. 2016) used by LVK to search for signals in gravitational-wave data all use ranking statistics in such a manner (Abbott et al. 2019b). Both PyCBC and GstLAL's ranking statistic incorporate information about the relative likelihood that the data contains a coherent signal versus noise. In contrast, cWB's ranking statistic uses the information of coherent energy present in the network of detectors (Abbott et al. 2019b).

Bayesian inference offers an alternative means to rank the significance of candidate events by computing the odds that the data contain a transient gravitational-wave signal versus instrumental glitches (Isi et al. 2018). This method relies on accurate models for the signal and glitch morphologies (Isi et al. 2018). In principle, Bayesian odds is the optimal method for hypothesis testing (Ashton et al. 2019b). Much of its power comes from the Bayesian evidence, the likelihood of the data given a hypothesis. However, the evidence is not used in current matched filter searches. Here, we explore a hybrid frequentist/Bayesian ranking statistic that makes use of the Bayesian evidence. We compute the Bayesian evidence under the assumption that the data either contain a coherent gravitational-wave signal, noise, or a glitch (Z^S, Z^N, Z^G, defined in Appendix A). However, because we do not have at our disposal a set of PyCBC triggers generated for simulated signals from a realistic population, we use the evidences as a ranking statistic, instead of computing true Bayesian odds. We form a bootstrapped distribution of the evidence for simulated foreground and background events to form a frequentist ranking statistic. Our work highlights the importance of an astrophysically realistic injection set for calculating $p_{\rm astro}$.

2.2 Formalism

Introduced by Isi et al. (2018), the Bayesian Coherence Ratio for a signal in a network of D detectors is given by

$$\rho_{\rm BCR} = \frac{\hat{\pi}^S Z^S}{\prod_{i=1}^{D} \left[\hat{\pi}_i^G Z_i^G + \hat{\pi}_i^N Z_i^N\right]}, \tag{1}$$

where $\{\hat{\pi}^S, \hat{\pi}_i^N, \hat{\pi}_i^G\}$ are 'pseudo prior probabilities' that the data contain a coherent signal, incoherent noise, or an incoherent glitch. These factors are not true prior probabilities because they are not chosen a priori. Rather, these factors are obtained by minimizing the overlap between a signal and background distribution (see Appendix D). We assume each detector has the same glitch and noise prior probabilities of $\{\hat{\pi}^N, \hat{\pi}^G\}$. In the limit where our pseudo prior probabilities equal the actual prior probabilities, the $\rho_{\rm BCR}$ becomes the optimal Bayesian odds described by Ashton et al. (2019b). However, as we do not (in this work) have a reliable estimate for the prior probabilities, we cannot interpret the $\rho_{\rm BCR}$ as a Bayesian odds to discriminate signals from glitches. Instead, we use the $\rho_{\rm BCR}$ as a ranking statistic to obtain a frequentist significance of $\rho_{\rm BCR}$.

Since it is impossible to shield ground-based gravitational-wave detectors from gravitational-wave signals, the LVK empirically estimates the background by repeatedly time-shifting strain data by amounts larger than the light-traveltime between the two LIGO detectors (Abbott et al. 2019b). We use time-shifted data to generate $\rho^b_{\rm BCR}$, the background ranking statistic. Following this, we calculate the fraction of $\rho^b_{\rm BCR}$ greater than or equal to a $\rho^c_{\rm BCR}$, the candidate

[1] 170222 is a sub-threshold candidate detected by PyCBC (SNR ~ 7.7). The prefix of GW is not utilized as this is a candidate event.

Table 1. Trigger-selection lab-frame parameter space (parameters correspond to signals with durations ≤454 ms and $q \geq 0.1$).

	Minimum	Maximum
Component mass 1, m_1 [$M_\odot$]	31.54	491.68
Component mass 2, m_2 [$M_\odot$]	1.32	121.01
Total mass, M [$M_\odot$]	56.93	496.72
Chirp mass, $\mathcal{M}$ [$M_\odot$]	8.00	174.56
Mass ratio, q	0.1	0.98

ranking statistic

$$p_1^b = \frac{\text{Count of } \rho^b_{\rm BCR} \leq \rho^c_{\rm BCR}}{\text{Count of } \rho^b_{\rm BCR}} \,. \tag{2}$$

Given a set of simulated signals and their ranking statistic $\rho^s_{\rm BCR}$, one may calculate the fraction of $\rho^s_{\rm BCR}$ greater than or equal to a $\rho^c_{\rm BCR}$

$$p_1^s = \frac{\text{Count of } \rho^s_{\rm BCR} \leq \rho^c_{\rm BCR}}{\text{Count of } \rho^s_{\rm BCR}} \,. \tag{3}$$

With p_1^b and p_1^s, it is possible to compute a candidate's $p_{\rm astro}$, the probability that a candidate is of astrophysical origin

$$p_{\rm astro} = \frac{p_1^s}{p_1^s + p_1^b} \,. \tag{4}$$

However, for this study, we do not have an astrophysical distribution of simulated signals and so we cannot compute p_1^s or consequently $p_{\rm astro}$. Instead, we opt for a frequentist p-value probability that a candidate is inconsistent with the background. As we have k candidates, each with a $\rho^c_{\rm BCR}$, we calculate a false-alarm probability p_B that accounts for trial factors given by

$$p_B = 1 - \left(1 - p_1^b\right)^k \,. \tag{5}$$

Finally, we compute the probability that a candidate is inconsistent with the background

$$p_{\bar{B}} = 1 - p_B \,. \tag{6}$$

When $p_{\bar{B}} \ll 1$, the event is consistent with the background distribution. Conversely, when $p_{\bar{B}} \approx 1$, the event is inconsistent with the background distribution, and is therefore a promising gravitational-wave candidate.

It is important to note that $p_{\bar{B}}$ (the probability that an event is not part of the background distribution) is not the same as $p_{\rm astro}$, which requires an astrophysical set of simulated signals.

3 ANALYSIS

We acquire candidate signal triggers (times when the detector's data has a signal-to-noise ratio above a predetermined threshold) for $\rho_{\rm BCR}$ analysis from PyCBC's search in O2 (Allen 2005; Allen et al. 2012; Dal Canton et al. 2014; Usman et al. 2016; Nitz et al. 2017, 2018, 2020a; Abbott et al. 2020b; Davies et al. 2020). Some of the triggers are associated with gravitational-wave events and candidates while others are glitches. We also acquire background time-slid triggers and simulated triggers from PyCBC's O2 search to calculate $\rho^b_{\rm BCR}$ and estimate values for $\{\hat{\pi}^S, \hat{\pi}^G\}$ (see Appendix B for details on the estimation process). The triggers are divided into 2-week time-frames because the detector's sensitivity does not stay constant throughout the 8-month-long observing period (Usman et al. 2016).

For our study, we filter PyCBC triggers to include only those in the parameter ranges presented in Table 1. This region focuses our analysis on binary black hole mergers with lab-frame total masses above $\gtrsim 55 M_\odot$, corresponding to binary systems with signal durations < 454 ms and $q \geq 0.1$. The filtering process leaves us with ∼70 000 background, ∼5000 simulated, and 25 candidate signal triggers. We additionally include events and candidate events reported by GWTC-1 and the IAS group in our list of candidate signal triggers. A plot of the lab-fame component mass space constrained by our search space is presented in Fig. 1.

To evaluate $\{Z^S, Z^G_i, Z^N_i\}$ and calculate the $\rho_{\rm BCR}$ (equation 1) for triggers, we carry out Bayesian inference with BILBY (Ashton et al. 2019a, 2020), employing DYNESTY (Speagle 2020) as our nested sampler. Nested sampling, an algorithm introduced by Skilling (2004, 2006), provides an estimate of the Bayesian evidence and is often utilized for parameter estimation within the LIGO collaboration (Ashton et al. 2019a, c; Smith et al. 2020).

We use a likelihood that marginalizes over coalescence time, the phase at coalescence, and luminosity distance (see Thrane & Talbot 2019, equation 80). We use identical parameter estimation priors for the glitch and signal models. We restrict the spin priors to aligned spins to reduce the number of parameters we sample. We define our mass priors to be uniform in chirp mass $\mathcal{M}$ and mass ratio q to avoid sampling issues that arise from sampling in thin regions of the component mass parameter space (Romero-Shaw et al. 2020a). As a post-processing step, we convert posterior samples calculated with uniform $\{\mathcal{M}, q\}$ priors to uniform component mass priors by re-sampling the posterior samples using the Jacobian given in Veitch et al. (2015, equation 21). The complete list of the priors is in Table 2.

The waveform template we utilize is `IMRPhenomPv2`, a phenomenological waveform template constructed in the frequency domain that models the in-spiral, merger, and ring-down (IMR) of a CBC (Khan et al. 2016). Although there exist gravitational-wave templates such as `IMRPhenomXPHM` (Pratten et al. 2020), `NRSur7dq4` (Blackman et al. 2017), and `SEOBNRv4PHM` (Ossokine et al. 2020) which incorporate more physics, such as information on higher order modes, we use `IMRPhenomPv2` as it is computationally inexpensive compared to others.

To generate the power spectral density (PSD), we take 31 neighbouring off-source non-overlapping 4-s segments of time-series data before the analysis data segment d_i. A Tukey window with a 0.2-s roll-off is applied to each data segment to suppress spectral leakage. After this, we fast-Fourier transform and median-average the segments to create a PSD (Abbott et al. 2020a). Like other PSD estimation methods, this method adds statistical uncertainties to the PSD (Chatziioannou et al. 2019; Biscoveanu et al. 2020; Talbot & Thrane 2020). To marginalize over the statistical uncertainty, we use the median-likelihood presented by Talbot & Thrane (2020) as a post-processing step. This post-processing step reduces the percentage of background $\rho^b_{\rm BCR} > 0$ by ∼ 49 per cent. The details of this calculation are in the Appendix C.

The data we use are the publicly accessible O2 strain data from the Hanford and Livingston detectors, recorded while the detectors are in 'Science Mode'. We obtain the data from the gravitational-wave Open Science Center (Abbott et al. 2021b) using GWPY (Macleod et al. 2020).

Finally, with the $\rho^c_{\rm BCR}$ and $\rho^b_{\rm BCR}$ for each time-frame of triggers, we calculate the candidate signal's $p_{\bar{B}}$.

4 RESULTS

We analyse the O2 candidates with $M > 55\,M_\odot$ and report candidates with $p_{\bar{B}} \geq 0.2$ in Table 3. The $\hat{\pi}^S$ and $\hat{\pi}^G$ values utilized for

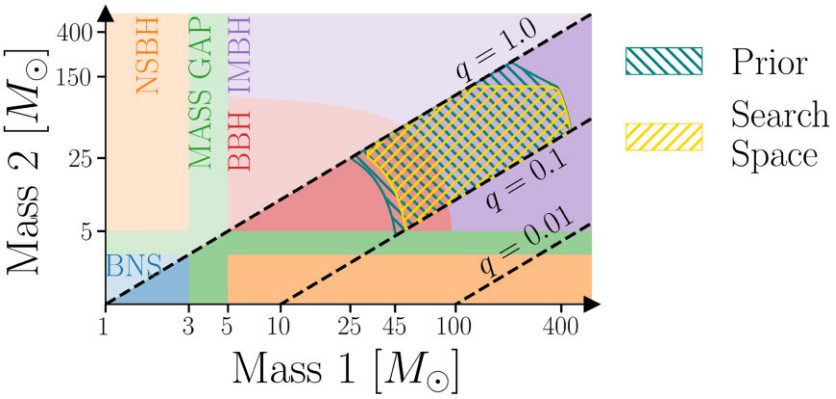

Figure 1. Lab-frame black hole component-mass boundaries for our search space and parameter estimation prior. Our search is constrained to the parameter space enclosed by the gold-coloured hatches, while our prior is constrained to the slightly larger parameter space enclosed by the teal-coloured hatches. The purple region labelled 'IMBH' is the parameter space where merger remnants may be IMBHs.

Table 2. Prior settings for the lab-frame parameters used during our parameter estimation. The definitions of the parameters are documented in Romero-Shaw et al. (2020a, Table E1). The trigger time t_c is obtained from the data products of PyCBC's O2 search.

Parameter	Shape	Limits
$\mathcal{M}$ ($M_\odot$)	Uniform	7–180
q	Uniform	0.1–1
M ($M_\odot$)	Constraint	50–500
d_L (Mpc)	Comoving	100–5000
χ_1, χ_2	Uniform	−1 to 1
θ_{JN}	Sinusoidal	0–π
ψ	Uniform	0–π
ϕ	Uniform	0–2π
RA	Uniform	0–2π
Dec.	Cosine	0–2π
t_c (s)	Uniform	$t_c \pm 0.1$

each time-frame are reported in Appendix D. By imposing a $p_{\bar{B}}$ threshold of 0.5, we present 13 candidate gravitational wave events.

Various search pipeline $p_{\rm astro}$ are not mathematically equivalent (Galaudage, Talbot & Thrane 2020). Moreover, $p_{\rm astro}$ is not equivalent to $p_{\bar{B}}$. However, by comparing candidates' various $p_{\rm astro}$ values with $p_{\bar{B}}$, we can compare how significant each pipeline deems the candidate. For comparison, in Table 3, we report $p_{\rm astro}$ values from GWTC-1 (Abbott et al. 2019b), PyCBC OGC-2 (Nitz et al. 2020b), PyCBC OGC-3 (Nitz et al. 2020b), IAS (Venumadhav et al. 2019; Zackay et al. 2021), and Pratten & Vecchio (2020)'s analyses.

4.1 GWTC-1 events

All the confirmed gravitational-wave events from binary black hole mergers reported in GWTC-1 and within our prior space (specifically GW170104, GW170608, GW170729, GW170809, and GW170814) have $p_{\bar{B}} > 0.9$, indicating a high probability of an astrophysical signal.

In addition to the above confirmed gravitational-wave events from GWTC-1, we have also analysed several candidate events from GWTC-1, most of which have low $p_{\bar{B}}$. For example, consider the candidate event 170412 ($t_c = 1176047817$), assigned a $p_{\rm astro}$ of 0.06 by GstLAL and has a $p_{\bar{B}}$ of 0.01. This candidate was reported to be excess power caused due to noise appearing non-stationary between 60 and 200 Hz (Abbott et al. 2019b). This candidate demonstrates that $p_{\bar{B}}$ may be utilized to eliminate candidates originating from terrestrial noise sources.

4.2 IAS events

Our analysis of the IAS events and candidates with $M \gtrsim 55$ $M_\odot$ in O2 has resulted in one event with disfavoured $p_{\bar{B}} < 0.5$ (GW170425), and five events and two candidates with $p_{\bar{B}} \geq 0.5$ (GW170121, GW170304, 170302, GWC170402, GW170403, GW170727, GW170817A). From this list, four events (GW170121, GW170304, GW170727, GW170817A) have $p_{\bar{B}} > 0.8$ and $p_{\rm astro} > 0.9$ reported from other pipelines, making them viable gravitational-wave event candidates.

GWC170402, detected by Zackay et al. (2021), is reported to originate from a binary with non-zero eccentricity (Zackay et al. 2021). As we used a non-eccentric waveform during analysis, we may be under estimating this event's significance at $p_{\bar{B}} \leq 0.6$. Finally, GW170425 which has $p_{\bar{B}} < 0.25$ also has low $p_{\rm astro}$ reported in OGC-2 and OGC-3 (Nitz et al. 2020b, 2021), suggesting that GW170425 may have been a false alarm.

4.3 New candidate events

Although no IMBH detections are made with the $\rho_{\rm BCR}$, a marginal stellar mass black hole merger candidate 170222 has been discovered with a $p_{\bar{B}} \sim 0.6$. This candidate has a SNR $\sim$ 7.7, low spin magnitudes, and source-frame component masses of $(47.16^{+8.00}_{-5.77}, 35.50^{+5.79}_{-6.35})M_\odot$ (90 per cent credible intervals), making it one of the heavier black hole mergers from O2 and GWTC-1. This candidate may be of interest as one component black hole may lie in the pair-instability mass gap $(55^{+10}_{-10} - 148^{+13}_{-12})M_\odot$ (Heger & Woosley 2002; Woosley & Heger 2021). More details on the candidate are presented in Appendix E. The remaining coherent trigger candidates all have $p_{\bar{B}} < 0.5$, making them unlikely to originate from astrophysical sources.

5 CONCLUSION

In this paper, we demonstrate that the Bayesian Coherence Ratio $\rho_{\rm BCR}$ (Isi et al. 2018) can be used as a ranking statistic to provide a measure of significance for gravitational-wave signals originating

Table 3. $p_{\bar{B}}$ table for gravitational wave events and candidates in our search space with $p_{\bar{B}} > 0.2$, calculated using Hanford and Livingston observatory data. Displayed for comparison are significances of events taken from: GstLAL $p_{\rm astro}^{\rm GstLAL}$ (Abbott et al. 2019b), PyCBC $p_{\rm astro}^{\rm pyCBC}$ (Abbott et al. 2019b), IAS $p_{\rm astro}^{\rm IAS}$ (Venumadhav et al. 2019; Zackay et al. 2021), $P(S|{\rm d})$ (Pratten & Vecchio 2020), PyCBC OGC-2 $p_{\rm astro}^{\rm OGC2}$ (Nitz et al. 2020b), and PyCBC OGC-3 $p_{\rm astro}^{\rm OGC3}$ (Nitz et al. 2020b). The t_c column contains the 'GPS' coalescence-times of the gravitational wave events. The catalogue column displays the first catalogue reporting the event on each row (the catalogues labeled IAS-1 and IAS-2 correspond to the candidates published by Venumadhav et al. 2019 and Zackay et al. 2021).

Event	Catalogue	$p_{\bar{B}}$	$p_{\rm astro}^{\rm pyCBC}$	$p_{\rm astro}^{\rm GstLAL}$	$p_{\rm astro}^{\rm IAS}$	$P(S\|{\rm d})$	$p_{\rm astro}^{\rm OGC2}$	$p_{\rm astro}^{\rm OGC3}$	t_c
GW170104	GWTC-1	0.97	1.00	1.00		1.00	1.00		1167559936.60
GW170121	IAS-1	0.83			1.00	0.53	1.00	1.00	1169069154.57
170209	–	0.32							1170659643.47
170222	–	0.58							1171814476.97
170302	IAS-1	0.78			0.45				1172487817.48
GW170304	IAS-1	0.94			0.99	0.03	0.70	0.70	1172680691.36
GWC170402	IAS-2	0.60			0.68	0.00			1175205128.57
GW170403	IAS-1	0.54			0.56	0.27	0.03	0.71	1175295989.22
170421	–	0.27							1176789158.14
GW170425	IAS-1	0.22			0.77	0.74	0.21	0.41	1177134832.18
GW170608	GWTC-1	0.99	1.00	0.92		1.00			1180922494.50
GW170727	IAS-1	0.98			0.98	0.66	0.99	1.00	1185152688.02
GW170729	GWTC-1	0.98	0.52	0.98		1.00	1.00	0.99	1185389807.30
GW170809	GWTC-1	0.99	1.00	0.99		1.00	1.00	1.00	1186302519.75
GW170814	GWTC-1	1.00	1.00	1.00		1.00	1.00	1.00	1186741861.53
GW170817A	IAS-2	0.92			0.86	0.02			1186974184.72

from CBCs with lab-frame total masses between 55 $M_\odot$ and 400 $M_\odot$, a range that includes IMBHs. To compute the $\rho_{\rm BCR}$ for candidates, we utilize Bayesian inference to calculate the probability of data under various hypotheses (the hypotheses that the data contains a coherent signal, just noise, or an incoherent glitch). This Bayesian ranking method takes a step towards building a unified Bayesian framework that provides a measure of significance for candidates and estimates their parameters, utilizing the same level of physical information incorporated during detected parameter estimation studies.

In our study, we analyse O2 binary-black hole events and candidates with $M > 55\,M_\odot$ reported by the PyCBC search (Nitz et al. 2020b), the IAS-team (Venumadhav et al. 2019; Zackay et al. 2021) and those reported in GWTC-1 (Abbott et al. 2019b). Using a $p_{\bar{B}}$ threshold of 0.5, we find that the GWTC-1 events have high probabilities of originating from an astrophysical source. We also find that some of the GWTC-1 marginal triggers that have corroborated terrestrial sources (for example, candidate 170412) have low $p_{\bar{B}}$, indicating this method's ability to discriminate between terrestrial artifacts and astrophysical signals. Our analysis of the IAS events demonstrates that GW170121, GW170304, GW170727, and GW170817A are likely to originate from astrophysical sources ($p_{\bar{B}} \geq 0.8$), while GW170425 is not ($p_{\bar{B}} < 0.25$). Finally, we report a new marginal binary-black hole merger candidate, 170222.

With the rapid rate of development in gravitational-wave Bayesian inference, we anticipate the ability to analyse longer duration signals, utilize more advanced signal and glitch models, and incorporate data from the entire detector network. In a similar vein, with the accumulation of more gravitational wave events, future $\rho_{\rm BCR}$ work may utilize astrophysically informed priors during Bayesian inference and more accurate prior probabilities for each detector.

ACKNOWLEDGEMENTS

The authors gratefully thank the PyCBC team for providing the gravitational-wave foreground, background, and simulated triggers from PyCBC's search of O2's data. We also warmly thank Ian Harry and Thomas Dent for answering questions about the PyCBC search's data products.

We gratefully acknowledge the computational resources provided by the LIGO Laboratory-Caltech Computing Cluster and supported by NSF grants PHY-0757058 and PHY-0823459, and thank Stuart Anderson for his assistance in resource scheduling.

All analyses (inclusive of test and failed analyses) performed for this study used 0.6 M core-hours, amounting to a carbon footprint of ~77 t of CO_2 [using the US average electricity source emissions of 0.371 kg kWh^{-1} (Carbonfund.org 2020) and 0.3 kWh for each CPU].

This material is based upon work supported by NSF's LIGO Laboratory, a major facility fully funded by the National Science Foundation. This research has used data, software, and web tools obtained from the Gravitational Wave Open Science Center (https://www.gw-openscience.org), a service of LIGO Laboratory, the LIGO Scientific Collaboration, and the Virgo Collaboration. LIGO Laboratory and Advanced LIGO are funded by the United States National Science Foundation (NSF) as well as the Science and Technology Facilities Council (STFC) of the United Kingdom, the Max-Planck-Society (MPS), and the State of Niedersachsen/Germany for support of the construction of Advanced LIGO and construction and operation of the GEO600 detector. Additional support for Advanced LIGO was provided by the Australian Research Council. Virgo is funded, through the European Gravitational Observatory (EGO), by the French Centre National de Recherche Scientifique (CNRS), the Italian Istituto Nazionale di Fisica Nucleare (INFN), and the Dutch Nikhef, with contributions by institutions from Belgium, Germany, Greece, Hungary, Ireland, Japan, Monaco, Poland, Portugal, and Spain.

DATA AVAILABILITY

We analyse publicly available gravitational wave strain data from the LIGO-Virgo-KAGRA collaboration (Gravitational Wave Open Science Center 2019). The trigger times for analysis were provided

by the PyCBC team (Nitz et al. 2020b). The derived data generated in this research will be shared on reasonable request to the corresponding author.

Software: BILBY (v0.6.8; Ashton et al. 2019a), BILBY-PIPE (v0.3.12; Ashton et al. 2020), DYNESTY (v0.9.5.3; Speagle 2020), GWPY (v1.0.1; Macleod et al. 2020), LALSIMULATION (v6.70; LIGO Scientific Collaboration 2018), MATPLOTLIB (v3.2.0; Hunter 2007), NUMPY (v1.8.1; Harris et al. 2020), SCIPY (v1.4.1; Virtanen et al. 2020), PANDAS (v1.0.2; Reback et al. 2020), PYTHON (v3.7; Oliphant 2007; Millman & Aivazis 2011).

REFERENCES

Abbott B. P. et al., 2019a, Phys. Rev. D, 100, 064064
Abbott B. P. et al., 2019b, Phys. Rev. X, 9, 031040
Abbott B. P. et al., 2020a, Class. Quantum Gravity., 37, 055002
Abbott R. et al., 2020b, available at: dcc.ligo.org/P1900392
Abbott R. et al., 2020c, Phys. Rev. Lett., 125, 101102
Abbott B. P. et al., 2021a, Phys. Rev. X, 11, 021053
Abbott R. et al., 2021b, SoftwareX, 13, 100658
Abbott R. et al., 2022, A&A, 659, A84
Acernese F. et al., 2015, Class. Quantum Gravity, 32, 024001
Allen B., 2005, Phys. Rev. D, 71, 062001
Allen B., Anderson W. G., Brady P. R., Brown D. A., Creighton J. D. E., 2012, Phys. Rev. D, 85, 122006
Amaro-Seoane P., Gair J. R., Freitag M., Miller M. C., Mandel I., Cutler C. J., Babak S., 2007, Class. Quantum Gravity, 24, R113
Anagnostou O., Trenti M., Melatos A., 2020, PASA, 37, e044
Arca Sedda M., Mastrobuono-Battisti A., 2019, preprint (arXiv:1906.05864)
Ashton G., Thrane E., 2020, MNRAS, 498, 1905
Ashton G., Hübner M., Lasky P., Talbot C., 2019a, ApJS, 241, 27
Ashton G., Thrane E., Smith R. J. E., 2019b, Phys. Rev. D, 100, 123018
Ashton G. et al., 2019c, ApJS, 241, 27
Ashton G., Romero-Shaw I., Talbot C., Hoy C., Galaudage S., 2020, Bilby Pipe: 1.0.1. Available at: https://lscsoft.docs.ligo.org/bilby_pipe/master/index.html
Askar A., Davies M. B., Church R. P., 2021, MNRAS, 502, 2682
Balick B., Brown R. L., 1974, ApJ, 194, 265
Ballone A., Torniamenti S., Mapelli M., Di Carlo U. N., Spera M., Rastello S., Gaspari N., Iorio G., 2021, MNRAS, 501, 2920
Banerjee S., 2021a, MNRAS, 500, 3002
Banerjee S., 2021b, MNRAS, 503, 3371
Bellovary J. M., Mac Low M.-M., McKernan B., Ford K. E. S., 2016, ApJ, 819, L17
Biscoveanu S., Haster C.-J., Vitale S., Davies J., 2020, Phys. Rev. D, 102, 023008
Blackman J. et al., 2017, Phys. Rev. D, 96, 024058
Bouffanais Y., Mapelli M., Santoliquido F., Giacobbo N., Di Carlo U. N., Rastello S., Artale M. C., Iorio G., 2021, MNRAS, 507, 5224
Cabero M. et al., 2019, Class. Quantum Gravity, 36, 155010
Carbonfund.org, 2020, Carbon Fund
Chandra K., Villa-Ortega V., Dent T., McIsaac C., Pai A., Harry I. W., Cabourn Davies G. S., Soni K., 2021, Phys. Rev. D, 104, 042004
Chatziioannou K., Haster C.-J., Littenberg T. B., Farr W. M., Ghonge S., Millhouse M., Clark J. A., Cornish N., 2019, Phys. Rev. D, 100, 104004
Chu Q. et al., 2022, Phys. Rev. D, 105, 024023
Dal Canton T. et al., 2014, Phys. Rev. D, 90, 082004
Davies G. S., Dent T., Tápai M., Harry I., McIsaac C., Nitz A. H., 2020, Phys. Rev. D, 102, 022004
Event Horizon Telescope Collaboration et al., 2019, ApJ, 875, L1
Farrell E., Groh J. H., Hirschi R., Murphy L., Kaiser E., Ekström S., Georgy C., Meynet G., 2021, MNRAS, 502, L40
Freire P. C. C. et al., 2017, MNRAS, 471, 857
Galaudage S., Talbot C., Thrane E., 2020, Phys. Rev. D, 102, 083026
Genzel R., Eisenhauer F., Gillessen S., 2010, Rev. Mod. Phys., 82, 3121
Ghez A. M., Klein B. L., Morris M., Becklin E. E., 1998, ApJ, 509, 678
Graham A. W., Scott N., 2013, ApJ, 764, 151
Gravitational Wave Open Science Center, 2019, The O2 Data Release. Available at: https://doi.org/10.7935/CA75-FM95
Greene J. E., Ho L. C., 2004, ApJ, 610, 722
Greene J. E., Strader J., Ho L. C., 2020, ARA&A, 58, 257
Gröbner M., Ishibashi W., Tiwari S., Haney M., Jetzer P., 2020, A&A, 638, A119
Gürkan M. A., Fregeau J. M., Rasio F. A., 2006, ApJ, 640, L39
Harris C. R. et al., 2020, Nature, 585, 357
Heger A., Woosley S. E., 2002, ApJ, 567, 532
Hunter J. D., 2007, Comput. Sci. Eng., 9, 90
Inayoshi K., Hirai R., Kinugawa T., Hotokezaka K., 2017, MNRAS, 468, 5020
Ishibashi W., Gröbner M., 2020, A&A, 639, A108
Isi M., Smith R., Vitale S., Massinger T. J., Kanner J., Vajpeyi A., 2018, Phys. Rev. D, 98, 042007
Israel G. L. et al., 2017, MNRAS, 466, L48
Kanner J. B. et al., 2016, Phys. Rev. D, 93, 022002
Khan S., Husa S., Hannam M., Ohme F., Pürrer M., Forteza X. J., Bohé A., 2016, Phys. Rev. D, 93, 044007
Kızıltan B., Baumgardt H., Loeb A., 2017, Nature, 542, 203
Klimenko S. et al., 2016, Phys. Rev. D, 93, 042004
Koliopanos F., 2017, Proc. Sci., Intermediate Mass Black Holes: A Review. SISSA, Trieste, PoS(MULTIF2017)051
Kumamoto J., Fujii M. S., Trani A. A., Tanikawa A., 2021, MNRAS, preprint (arXiv:2102.09323)
LIGO Scientific Collaboration, 2018, Astrophysics Source Code Library, record ascl:2012.021
LIGO Scientific Collaboration et al., 2015, Class. Quantum Gravity, 32, 074001
Lin D. et al., 2020, ApJ, 892, L25
Liu B., Bromm V., 2020, MNRAS, 495, 2475
Lu X.-Y., Tan Y.-J., Shao C.-G., 2019, Phys. Rev. D, 100, 044042
McKernan B., Ford K. E. S., Lyra W., Perets H. B., 2012, MNRAS, 425, 460
McKernan B., Ford K. E. S., Kocsis B., Lyra W., Winter L. M., 2014, MNRAS, 441, 900
McKernan B. et al., 2018, ApJ, 866, 66
McKernan B. et al., 2019, ApJ, 884, L50
Macleod D. et al., 2020, Zenodo, gwpy/gwpy: 1.0.1. Available at: https://doi.org/10.5281/zenodo.3598469
Mapelli M. et al., 2021, MNRAS, 505, 339
Martinez M. A. S. et al., 2020, ApJ, 903, 67
Martynov D. V. et al., 2016, Phys. Rev. D, 93, 112004
Mezcua M., 2017, Int. J. Mod. Phys. D, 26, 1730021
Millman K. J., Aivazis M., 2011, Comput. Sci. Eng., 13, 9
Moore C. J., Cole R. H., Berry C. P. L., 2014, Class. Quantum Gravity, 32, 015014
Nitz A. H., 2018, Class. Quantum Gravity, 35, 035016
Nitz A. H., Dent T., Dal Canton T., Fairhurst S., Brown D. A., 2017, ApJ, 849, 118
Nitz A. H., Dal Canton T., Davis D., Reyes S., 2018, Phys. Rev. D, 98, 024050
Nitz A. et al., 2020a, Zenodo, gwastro/pycbc: PyCBC Release 1.16.4. Available at: https://doi.org/10.5281/zenodo.3904502
Nitz A. H. et al., 2020b, ApJ, 891, 123
Nitz A. H., Dent T., Davies G. S., Harry I., 2020c, ApJ, 897, 169
Nitz A. H., Capano C. D., Kumar S., Wang Y.-F., Kastha S., Schäfer M., Dhurkunde R., Cabero M., 2021, ApJ, 922, 11
Oliphant T. E., 2007, Comput. Sci. Eng., 9, 10
Ossokine S. et al., 2020, Phys. Rev. D, 102, 044055
Paynter J., Webster R., Thrane E., 2021, Nat. Astron., 5, 560
Peterson B. M., 2014, Space Sci. Rev., 183, 253
Powell J., 2018, Class. Quantum Gravity, 35, 155017
Pratten G., Vecchio A., 2020, Phys. Rev. D, 104, 124039
Pratten G. et al., 2020, Phys. Rev. D, 103, 104056
Reback J. et al., 2020, Zenodo, pandas-dev/pandas: Pandas 1.0.2. Available at: https://doi.org/10.5281/zenodo.3708035
Ridolfi A. et al., 2016, MNRAS, 462, 2918
Rodríguez Castillo G. A. et al., 2020, ApJ, 895, 60

Romero-Shaw I. M. Ashton G. et al., 2020a, MNRAS, 499, 3295
Romero-Shaw I., Lasky P. D., Thrane E., Calderón Bustillo J., 2020b, ApJ, 903, L5
Sachdev S. et al., 2019, Phys. Rev. D, preprint (arXiv:1901.08580)
Safarzadeh M., Haiman Z., 2020, ApJ, 903, L21
Samsing J. et al., 2022, Nature, 603, 237
Schödel R. et al., 2002, Nature, 419, 694
Skilling J., 2004, in Fischer R., Preuss R., Toussaint U. V., eds, AIP Conf. Proc. Vol. 735, Bayesian Inference and Maximum Entropy Methods in Science and Engineering. Am. Inst. Phys., New York, p. 395
Skilling J., 2006, Bayesian Anal., 1, 833
Smith R. J. E., Ashton G., Vajpeyi A., Talbot C., 2020, MNRAS, 498, 4492
Speagle J. S., 2020, MNRAS, 493, 3132
Tagawa H., Haiman Z., Kocsis B., 2020, ApJ, 898, 25
Tagawa H., Kocsis B., Haiman Z., Bartos I., Omukai K., Samsing J., 2021, ApJ, 908, 194
Talbot C., Thrane E., 2020, Phys. Rev. Res., 2, 043298
Thrane E., Talbot C., 2019, PASA, 36, e010
Toubiana A. et al., 2021, Phys. Rev. Lett., 126, 101105
Usman S. A. et al., 2016, Class. Quantum Gravity, 33, 215004
Veitch J., Vecchio A., 2010, Phys. Rev. D, 81, 062003
Veitch J. et al., 2015, Phys. Rev. D, 91, 042003
Venumadhav T., Zackay B., Roulet J., Dai L., Zaldarriaga M., 2019, Phys. Rev. D, 100, 023011
Venumadhav T., Zackay B., Roulet J., Dai L., Zaldarriaga M., 2019, Phys. Rev. D, 101, 083030
Virtanen P. et al., 2020, Nature Meth., 17, 261
Weatherford N. C., Fragione G., Kremer K., Chatterjee S., Ye C. S., Rodriguez C. L., Rasio F. A., 2021, ApJ, 907, L25
Webster B. L., Murdin P., 1972, Nature, 235, 37
Wevers T., van Velzen S., Jonker P. G., Stone N. C., Hung T., Onori F., Gezari S., Blagorodnova N., 2017, MNRAS, 471, 1694
Woosley S. E., Heger A., 2021, ApJ, 912, L31
Yang Y. et al., 2019a, Phys. Rev. Lett., 123, 181101
Yang Y., Bartos I., Haiman Z., Kocsis B., Márka Z., Stone N. C., Márka S., 2019b, ApJ, 876, 122
Zackay B., Dai L., Venumadhav T., Roulet J., Zaldarriaga M., 2021, Phys. Rev. D, 104, 063030
Zevin M. et al., 2021, ApJ, 910, 152

APPENDIX A: BAYESIAN EVIDENCE EVALUATION

A1 Noise model

We assume that each detector's noise is Gaussian and stationary over the period being analysed (Abbott et al. 2020a). In practice, we assume that the noise has a mean of zero that the noise variance σ^2 is proportional to the noise power spectral density $P(f)$ of the data. Using $P(f)$, for each frequency-domain data segment d_i in each of the i detectors in a network of D detectors, we can write

$$Z_i^N = \mathcal{N}\left(d_i|\mu = 0, \sigma^2 = P(f)\right), \tag{A1}$$

where $\mathcal{N}$ is a normal distribution.

A2 Coherent signal model

We model coherent signals using a binary black hole waveform template $\mu(\vec{\theta})$, where the vector $\vec{\theta}$ contains a point in the 11-dimensional space describing aligned-spin binary-black hole mergers. For the signal to be coherent, $\vec{\theta}$ must be consistent in each 4-s data segment d_i for a network of D detectors. Hence, the coherent signal evidence is calculated as

$$Z^S = \int_{\vec{\theta}} \prod_{i=1}^{D} \left[\mathcal{L}(d_i|\mu(\vec{\theta}))\right] \pi(\vec{\theta}|\mathcal{H}_S)\, \mathrm{d}\vec{\theta}\,, \tag{A2}$$

where $\pi(\vec{\theta}|\mathcal{H}_S)$ is the prior for the parameters in the coherent signal hypothesis $\mathcal{H}_S$; and $\mathcal{L}(d_i|\mu(\vec{\theta}))$ is the likelihood for the coherent signal hypothesis that depends on the gravitational-wave template $\mu(\vec{\theta})$ and its parameters $\vec{\theta}$.

A3 Incoherent glitch model

Finally, as glitches are challenging to model and poorly understood, we follow Veitch & Vecchio (2010) and utilize a surrogate model for glitches. The glitches are modelled using gravitational-wave templates $\mu(\vec{\theta})$ with uncorrelated parameters amongst the different detectors such that $\vec{\theta}_i \neq \vec{\theta}_j$ for two detectors i and j (Veitch & Vecchio 2010). Modelling glitches with $\mu(\vec{\theta})$ captures the worst-case scenario: when glitches are identical to gravitational-wave signals (excluding coherent signals). Thus, we can write Z_i^G as

$$Z_i^G = \int_{\vec{\theta}} \mathcal{L}(d_i|\mu(\vec{\theta}))\, \pi(\vec{\theta}|\mathcal{H}_G)\, \mathrm{d}\vec{\theta}\,, \tag{A3}$$

where $\pi(\theta|\mathcal{H}_G)$ is the prior for the parameters in the incoherent glitch hypothesis $\mathcal{H}_G$.

APPENDIX B: TUNING THE PRIOR PROBABILITIES

After calculating the $\rho_{\rm BCR}$ for a set of background triggers and simulated triggers from a stretch of detector-data (a data chunk), we can compute probability distributions for the background and simulated triggers, $p_b(\rho_{\rm BCR})$ and $p_s(\rho_{\rm BCR})$. We expect the background trigger and simulated signal $\rho_{\rm BCR}$ values to favour the incoherent glitch and the coherent signal hypothesis, respectively. Ideally, these distributions representing two unique populations should be distinctly separate and have no overlap in their $\rho_{\rm BCR}$ values. The prior probability parameters $\hat{\pi}^S$ and $\hat{\pi}^G$ from Equation 1 help separate the two distributions. Altering $\hat{\pi}^S$ translates the $\rho_{\rm BCR}$ probability distributions while adjusting $\hat{\pi}^G$ spreads the distributions (see Isi et al. 2018, Appendix A). Although Bayesian hyper-parameter estimation can determine the optimal values for $\hat{\pi}^S$ and $\hat{\pi}^G$, an easier approach is to adjust the parameters for each data chunk's $\rho_{\rm BCR}$ distribution. In this study, we tune $\hat{\pi}^S$ and $\hat{\pi}^G$ to maximally separate the $\rho_{\rm BCR}$ distributions for the background and simulated triggers.

To calculate the separation between $p_b(\rho_{\rm BCR})$ and $p_s(\rho_{\rm BCR})$, we use the Kullback–Leibler divergence (KL divergence) $D_{\rm KL}$, given by

$$D_{KL}(p_b|p_s) = \sum_{x\in\rho_{\rm BCR}} p_b(x) \log\left(\frac{p_b(x)}{p_s(x)}\right)\,. \tag{B1}$$

The $D_{\rm KL} = 0$ when the distributions are identical and increases as the asymmetry between the distributions increases.

We limit our search for the maximum KL-divergence in the $\hat{\pi}^S$ and $\hat{\pi}^G$ ranges of $[10^{-10}, 10^0]$. We set our values for $\hat{\pi}^S$ and $\hat{\pi}^G$ to those which provide the highest KL-divergence and calculate the $\rho_{\rm BCR}$ for candidate events present in this data chunk. Note that we conduct the analysis in data chunks of two weeks rather than an entire data set of a few months as the background may be different at different points of the entire data set.

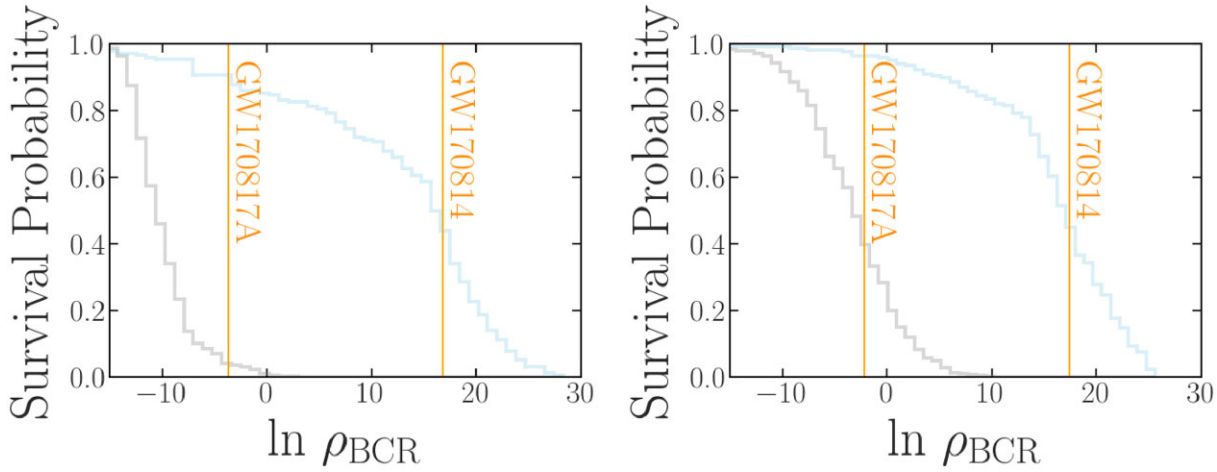

Figure C1. Histograms represent the survival function (1-CDF) from our selection of background triggers (grey) and simulated signals (blue) triggers obtained from PyCBC's search of data from 2017 August 13–21. Vertical lines mark the ln $\rho_{\rm BCR}$ of IAS's GW170817A and GWTC-1's GW170814. Left-hand panel: Survival functions using the post-processing step to marginalize over PSD statistical uncertainties. Right-hand panel: Survival functions without the post-processing step. Without the post-processing step, there is a greater overlap between the background (grey) and foreground (blue) survival functions.

APPENDIX C: MARGINALIZING OVER PSD STATISTICAL UNCERTAINTIES

To generate the results presented in Table 3, we applied a post-processing step to marginalize the uncertainty in the PSD. In Fig. C1, we demonstrate the impact of the post-processing step. Marginalizing over uncertainty in the PSD yields an improvement in the separation of the noise and signal distributions (left plot). Quantitatively, at a threshold ${\rho_{\rm BCR}}^T = 0$, the post-processing step reduces the percentage of background $\rho_{\rm BCR} > {\rho_{\rm BCR}}^T$ from 60 to 25 per cent (a 58 per cent improvement) in the August 13–21 time-frame of data. For the entirety of O2, PSD marginalization reduces the percentage of $\rho_{\rm BCR} > {\rho_{\rm BCR}}^T$ from 64 to 33 per cent (a $\sim$ 49 per cent improvement).

APPENDIX D: TUNED PRIOR PROBABILITIES

O2 lasted several months, over which the detector's sensitivity varied. Hence, a part of our analysis entailed tuning the prior probabilities for obtaining a signal and a glitch, $\hat{\pi}^S$ and $\hat{\pi}^G$, as described in Section 2. Table D1 presents the signal and glitch prior probabilities utilized for each time-frame of O2 data.

Tuning the prior probabilities can dramatically affect the $p_{\bar{B}}$. For example, consider Table D2, which reports tuned $p_{\bar{B}}$ and un-tuned $p'_{\bar{B}}$ (where $\hat{\pi}^S = 1$ and $\hat{\pi}^G = 1$) for various events and candidates. By tuning the prior probabilities, the $p_{\bar{B}}$ for some IAS events (for example, GW170403 and GW170817A) can change by more than 0.5, resulting in the promotion/demotion of a candidate's significance.

Table D1. The prior odds used for each time-frame of data from O2. Each time frame commences at the start date and concludes at the following time-frame's start date.

Start Date	$\hat{\pi}^S$	$\hat{\pi}^G$
2016-12-23	1.00E+00	6.25E–01
2017-01-22	1.00E+00	2.33E–02
2017-02-03	1.00E–10	2.44E–01
2017-02-12	1.76E–08	5.96E–02
2017-02-20	6.55E–10	2.22E–03

Table D1 – *continued*

Start Date	$\hat{\pi}^S$	$\hat{\pi}^G$
2017-02-28	1.00E–10	5.96E–02
2017-03-10	2.56E–10	3.91E–01
2017-03-18	1.60E–10	1.00E+00
2017-03-27	1.10E–08	5.96E–02
2017-04-04	3.73E–02	2.33E–02
2017-04-14	1.05E–09	2.44E–01
2017-04-23	2.68E–09	1.46E–02
2017-05-08	1.00E+00	2.44E–01
2017-06-18	6.55E–10	3.39E–04
2017-06-30	2.02E–05	5.69E–03
2017-07-15	1.05E–09	9.54E–02
2017-07-27	1.00E+00	2.12E–04
2017-08-05	2.12E–04	3.73E–02
2017-08-13	2.68E–09	8.69E–04

Table D2. Table of $p_{\bar{B}}$ using 'tuned' prior odds and $p_{\bar{B}}$ using uninformed prior odds of $\hat{\pi}^S = 1$ and $\hat{\pi}^G = 1$ (represented by $p'_{\bar{B}}$). Details of other columns are provided in Table 3.

Event	Catalogue	$p_{\bar{B}}$	$p'_{\bar{B}}$	t_c
GW170104	GWTC-1	0.97	0.95	1167559936.60
GW170121	IAS-1	0.83	0.68	1169069154.57
170209	–	0.32	0.00	1170659643.47
170222	–	0.58	0.50	1171814476.97
170302	IAS-1	0.78	0.54	1172487817.48
GW170304	IAS-1	0.94	0.80	1172680691.36
GWC170402	IAS-2	0.60	0.00	1175205128.57
GW170403	IAS-1	0.54	0.90	1175295989.22
170421	–	0.27	0.21	1176789158.14
GW170425	IAS-1	0.22	0.16	1177134832.18
GW170608	GWTC-1	0.99	0.99	1180922494.50
GW170727	IAS-1	0.98	0.99	1185152688.02
GW170729	GWTC-1	0.98	0.95	1185389807.30
GW170809	GWTC-1	0.99	0.99	1186302519.75
GW170814	GWTC-1	1.00	1.00	1186741861.53
GW170817A	IAS-2	0.92	0.30	1186974184.72

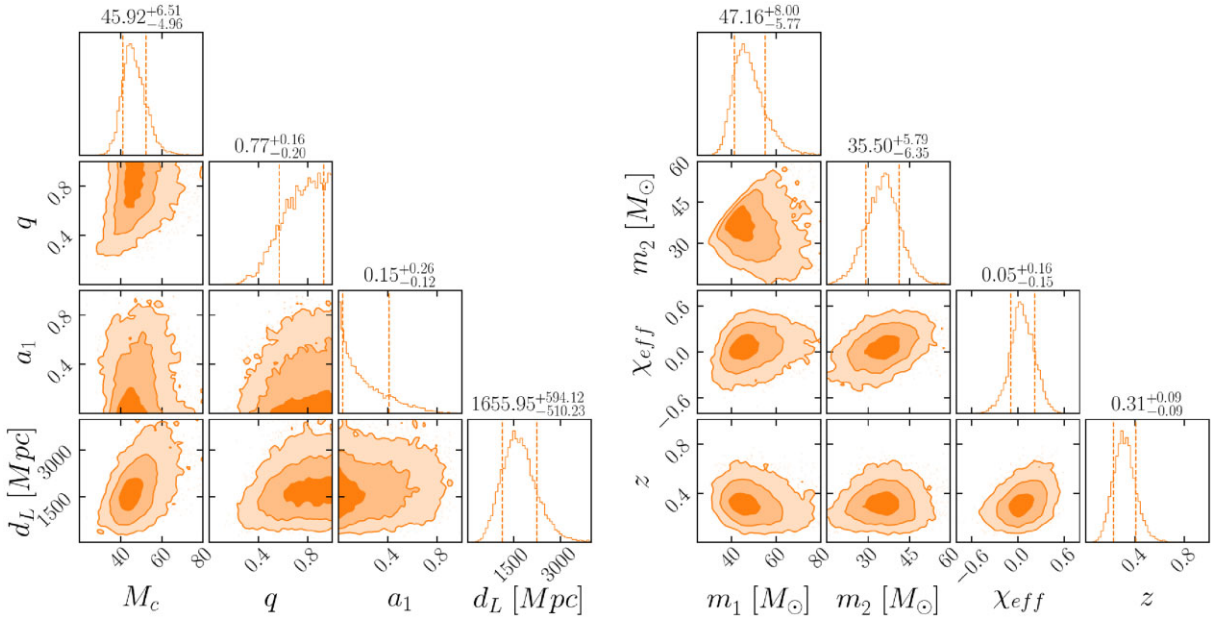

Figure E1. Posterior distributions for eight parameters of 170 222. Left-hand panel: Posterior probability distributions for 4 of the 12 search parameters. Right-hand panel: Posterior probability distributions for four derived parameters.

APPENDIX E: A CLOSER LOOK AT 170222

PyCBC found the candidate 170 222 with $\mathcal{M} = 49.46\ \mathrm{M}_\odot$ and $q = 0.68$, values contained inside the 90 per cent credible intervals of our posterior probability distributions for 170 222. Some of the posteriors produced as a by-product of our ρ_{BCR} calculation can be viewed in Fig. E1.

This paper has been typeset from a TEX/LATEX file prepared by the author.